Journal of Advanced Scientific Research
Available online through https://sciensage.info
ISSN
0976-9595
Research Article

ANTIMICROBIAL ACTIVITY, MOLECULAR DOCKING, SPECTROSCOPIC, DFT AND VIBRATIONAL ANALYSIS ON 3-(4 BROMOPHENYL)-1-METHOXY-1-METHYL UREA

P. R. Babila[1], E. S. Ashlin[2], G. Edwin Sheela*[3]

[1]*Research Scholar, Reg.No:19123092132011, Department of Physics and Research centre, Muslim Arts College, Thiruvinthancode-Tamilnadu, India (Affiliated to Manonmaniam Sundaranar University, Tirunelveli, Abishekapatti, Tamilnadu, India)*

[2]*Research Scholar,Reg.No:19123092132010, Department of Physics and Research centre, Muslim Arts College, Thiruvinthancode-Tamilnadu, India (Affiliated to Manonmaniam Sundaranar University, Tirunelveli, Abishekapatti, Tamilnadu, India)*

[3]*Department of Physics and Research centre, Muslim Arts College, Thiruvinthancode-Tamilnadu, India (Affiliated to Manonmaniam Sundaranar University, Tirunelveli, Abishekapatti, Tamilnadu, India)*

**Corresponding author: prbabila@gmail.com*

Received: 28-04-2022; Accepted: 07-06-2022; Published: 30-06-2022

© Creative Commons Attribution-NonCommercial-NoDerivatives 4.0 International License https://doi.org/10.55218/JASR.202213505

ABSTRACT

The main objective of the study is to analyze the spectral behaviour and antimicrobial activity of 3-(4 bromophenyl)-1-methoxy-1-methyl urea by experiment, theoretical spectroscopic, IR, Raman and UV-Vis techniques. The optimized geometrical parameters were reported on DFT/B3LYP/6-311++G (d, p) basis set of theory. Based on the potential distribution of energy, the detailed vibrational assignments of observed FT-IR and FT-Raman bands have been proposed. The distribution of vibrational modes was carried out by using normal coordinate analysis. Antimicrobial activity of BMM molecule was confirmed using molecular docking analysis. *In vitro* antimicrobial studies were carried out against the bacterial strains *E. coli* and *Candida* sp.

Keywords: DFT, BMM, NBO, MEP, NLO.

1. INTRODUCTION

The 3-(4 bromophenyl)-1-methoxy-1-methyl urea (BMM) belongs to the urea class and is classified in Herbicide Resistance Action Committee (HRAC) point group C_1 and inhibits photosynthesis [1]. Because of its severe bio-toxicity and probable carcinogenic qualities, BMM, the phenyl urea herbicide family, attracts special attention [2]. It is commonly used as a weed killer, to control unwanted plants. The molecular formula for BMM is $C_9H_{11}BrN_2O_2$ and its molecular mass is 259.1 g/mol. It has an asymmetric top molecule. The concentration of BMM is affected by a variety of conditions, including rainfall, temperature, and antifungal action [3]. In order to determine the physicochemical qualities responsible for the molecules stability, a complete structural study was performed utilizing theoretical and experimental data.

2. EXPERIMENTAL

2.1. Material and procedure

BMM is a faint beige color powder sample that was acquired from Sigma Aldrich Chemical Company with a starting purity of greater than 98 percent was utilized. The BMM molecule FT-IR spectrum was acquired using a KBr pellet at room temperature in a PERKIN ELMER spectrophotometer with a spectral resolution of 1.0 cm^{-1}. The compound FT-Raman spectrum was also recorded in an Nd: YAG laser using a BRUCKER RFS 27 with 200 Mw and a spectral resolution of 2 cm^{-1}. The BMM molecule FT-IR and FT-Raman spectra were captured in the 4000-400 cm^{-1} and 4000-100 cm^{-1} range respectively. BMM molecule UV-visible absorption spectra was evaluated using a PERKIN ELMER LAMBDA 950 UV spectroscope. The antimicrobial activity of BMM molecule was analyzed by the well diffusion method against the bacterial strains *E.coli* and *Candida sp*.

2.2. Details of the computation

The electronic structural analysis and optimization geometry of the BMM molecule were accomplished using the Gaussian'09 software package and the DFT method with the 6-311++G (d, p) basis set and Becke's three Lee Yang Parr gradient-corrected correlation functional

(B3LYP) [4]. The NBO analysis and Frontier molecular orbital analysis were completed with the aid of Gaussian'09 software [5] and visualized with the help of Gauss view software [6]. With the help of Normal Coordinates Analysis NCA, a complete set of internal coordinates has been understood in order to calculate PED for each normal mode [7]. The MOLVIB (7.0) application was used to assign vibrational assignments to the BMM molecule using potential energy distribution (PED) [8]. The B3LYP/6-311++G (d,p) basis set was finished with Global Reactivity Descriptors and Fukui functions. The binding energy and intermolecular energy data indicate that the title molecule has chemical and biological activity via inhibiting hydrolysis.

3. RESULTS AND DISCUSSION

3.1. Geometry Optimization

The bond length, bond angle and dihedral angle of the BMM molecule have been calculated using the B3LYP/6-311G++ (d, p) level basis set. Two electronegative oxygen atoms, two nitrogen atoms, and one bromine halogen make up BMMs twenty-five atoms.

Table 1: Optimized bond lengths and bond angles of BMM molecule

Bond lengths	B3LYP/6-311++(d, p) [Å]	Expt [Å]	Bond angles	B3LYP/6-311++G(d, p) [^{0}]	Expt. [^{0}]
C_1-C_2	1.3895	1.3801	C_2-C_1-C_6	121.0	120.4
C_1-C_6	1.4023	1.3882	C_2-C_1-H_{23}	119.1	119.8
C_1-H_{23}	1.0855	0.9504	C_6-C_1-H_{23}	119.8	119.8
C_2-C_3	1.3912	1.3792	C_1-C_2-C_3	119.2	119.2
C_2-H_{24}	1.0823	0.9501	C_1-C_2-H_{24}	120.1	120.4
C_3-C_4	1.3898	1.3804	C_3-C_2-H_{24}	120.6	120.4
C_3-Br_{25}	1.9188	1.9032	C_2-C_3-C_4	120.5	121.5
C_4-C_5	1.3932	1.3811	C_2-C_3-Br_{25}	119.6	118.9
C_4-H_{21}	1.0825	0.9501	C_4-C_3-Br_{25}	119.8	119.6
C_5-C_6	1.4007	1.3910	C_3-C_4-C_5	120.2	118.9
C_5-H_{22}	1.0791	0.9503	C_3-C_4-H_{21}	120.3	120.6
C_6-N_7	1.4069	1.4110	C_5-C_4-H_{21}	119.5	120.5
N_7-H_8	1.0100	0.8802	C_4-C_5-C_6	119.9	120.5
N_7-C_9	1.3719	1.3624	C_4-C_5-H_{22}	120.3	119.8
C_9-O_{10}	1.2183	1.2273	C_6-C_5-H_{22}	119.8	119.7
C_9-N_{11}	1.4126	1.3732	C_1-C_6-C_5	119.1	119.4
N_{11}-C_{12}	1.4608	1.4480	C_1-C_6-N_7	117.2	118.1
N_{11}-O_{16}	1.4224	1.4101	C_5-C_6-N_7	123.7	122.6
C_{12}-H_{13}	1.0956	0.9791	C_6-N_7-H_8	117.1	118.1
C_{12}-H_{14}	1.0875	0.9802	C_6-N_7-C_9	127.9	123.9
C_{12}-H_{15}	1.0904	0.9793	H_8-N_7-C_9	114.7	118.0
O_{16}-C_{17}	1.4336	1.4211	N_7-C_9-O_{10}	125.9	125.1
C_{17}-H_{18}	1.0933	0.9792	N_7-C_9-N_{11}	113.9	114.7
C_{17}-H_{19}	1.0906	0.9811	O_{10}-C_9-N_{11}	120.2	120.1
C_{17}-H_{20}	1.0934	0.9802	C_9-N_{11}-C_{12}	117.3	121.0
			C_9-N_{11}-O_{16}	114.1	114.6
			C_{12}-N_{11}-O_{16}	111.3	112.6
			N_{11}-C_{12}-H_{13}	111.4	109.5
			N_{11}-C_{12}-H_{14}	107.7	109.5
			N_{11}-C_{12}-H_{15}	109.1	109.5
			H_{13}-C_{12}-H_{14}	109.8	109.4
			H_{13}-C_{12}-H_{15}	109.6	109.5
			H_{14}-C_{12}-H_{15}	109.2	109.5
			N_{11}-O_{16}-C_{17}	109.9	108.6
			O_{16}-C_{17}-H_{18}	110.9	109.5
			O_{16}-C_{17}-H_{19}	105.3	109.5
			O_{16}-C_{17}-H_{20}	110.9	109.5
			H_{18}-C_{17}-H_{19}	110.4	109.4
			H_{18}-C_{17}-H_{20}	109.7	109.4

The optimized Molecular geometry of BMM using Gaussian '09 is presented in Fig 1. The optimized geometrical parameters were compared to the experimental value in Table 1 & 2. According to the DFT approach, the typical C-H and C-C bond lengths in the phenyl ring are 1.08 Å and 1.39 Å respectively. As a result of the resonance reaction, the N_7-C_9 (1.3719Å) bond length decreases from its actual value (1.48Å), revealing the double bond character [9]. The maximum bond length was C_3-Br_{25} (1.9188 Å) and the minimum bond length was N_7-H_8 (1.01 Å). The C_3-Br_{25} bond has a weaker bond and N_7-H_8 bond has a stronger bond. As a result of steric interaction [10], the bond angles C_5-C_6-N_7 (123.68 Å) and C_6-N_7-C_9 (127.95 Å) increase. This is owing to amide hydrogen repulsion with H_{23}, with the non-bond of H_{23}...H_8 (2.47574 Å). The BMM molecule's global minimum energy for optimization was found to be -3183.81 Hartrees. It predicts 427 cartesian basis functions, 65 alpha electrons, and 65 beta electrons in the title molecule optimized B3LYP/6-311G++ (d, p) basis set. The energy of nuclear repulsion is 1126.12 Hartrees.

In accordance with the dominating double bond character, the C-O bond is established for the carbonyl (C_9-O_{10}=1.22Å). The C-O double bond is very important for the vibrations and analyzes the biological characters of the molecule. The exo-angle O_{16}-C_{17}-H_{19} (105.34), N_{11}-C_{12}-H_{14} (107.68) varies significantly (3.66°, 1.32°) from the expected trigonal angle (109°). The bond angles N_{11}-C_{12}-H_{15}, H_{13}-C_{12}-H_{14}, H_{13}-C_{12}-H_{15}, H_{14}-C_{12}-H_{15}, N_{11}-O_{16}-C_{17} (109°) shows that they exhibit the degree of sp^2 character. The computed dihedral angles C_4-C_5-C_6-N_7 (179°), H_{22}-C_5-C_6-C_1 (179°), and H_{22}-C_5-C_6-C_1 (179°) reveal that the carbon atom is almost planar with respect to the phenyl ring.

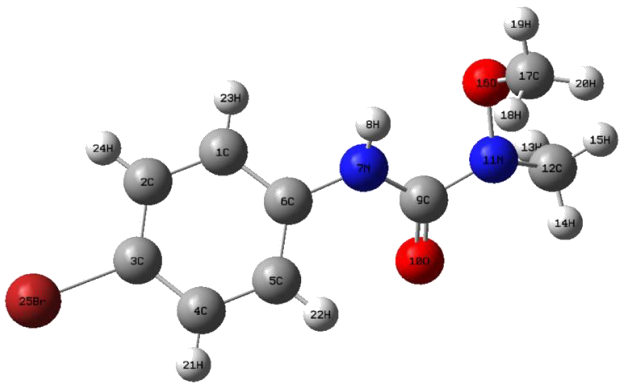


Fig. 1: Optimized molecular structure of BMM molecule

Table 2: Optimized dihedral angles of BMM molecule

Dihedral angles	B3LYP/6-311 ++G(d, p) [°]	Expt. [°]
C_6-C_1-C_2-C_3	-0.06	0.91
C_6-C_1-C_2-H_{24}	-179.99	-179.02
H_{23}-C_1-C_2-C_3	179.91	-179.11
H_{23}-C_1-C_2-H_{24}	-0.03	0.96
C_2-C_1-C_6-C_5	0.13	-2.78
C_2-C_1-C_6-N_7	-179.30	178.90
H_{23}-C_1-C_6-C_5	-179.84	177.24
H_{23}-C_1-C_6-N_7	0.73	-1.08
C_1-C_2-C_3-C_4	-0.02	1.47
C1-C2-C3Br_{25}	-179.98	-179.30
H_{24}-C_2-C_3-C_4	179.92	-178.60
H_{24}-C_2-C_3-Br_{25}	-0.04	0.62
C_2-C_3-C_4-C_5	0.02	-1.91
C_2-C_3-C_4-H_{21}	-179.89	178.06
Br_{25}-C_3-C_4-C_5	179.98	178.87
Br_{25}-C_3-C_4-H_{21}	0.07	-1.16
C_3-C_4-C_5-$_{C6}$	0.05	-0.02
C_3-C4-C_5-H_{22}	-179.52	179.99
H_{21}-C_4-C_5-C_6	179.96	-179.90
H_{21}-C_4-C_5-H_{22}	0.39	0.02
C_4-C_5-C_6-C_1	-0.13	2.33
C_4-C_5-C_6-N_7	179.27	179.43
H_{22}-C_5-C_6-C_1	179.45	-177.68
H_{22}-C_5-C_6-N_7	-1.15	0.56
C_1-C_6-N_7-H_8	-0.35	38.46
C_1-C_6-N_7-C_9	-174.53	141.54
C_5-C_6-N_7-H_8	-179.75	-139.81
C_5-C_6-N_7-C_9	6.06	40.19
C_6-N_7-C_9-O_{10}	2.54	-1.21
C_6-N_7-C_9-N_{11}	-174.71	-177.56
H_8-N_7-C_9-O_{10}	-171.75	178.79
H_8-N_7-C_9-N_{11}	10.99	2.44
N_7-C_9-N_{11}-C_{12}	-148.15	-157.80
N_7-C_9-N_{11}-O_{16}	-15.42	-17.58
O_{10}-C_9-N_{11}-C_{12}	34.42	25.65
O_{10}-C_9-N_{11}-O_{16}	167.15	165.87
C_9-N_{11}-C_{12}-H_{13}	77.47	66.07
C_9-N_{11}-C_{12}-H_{14}	-42.94	-53.90
C_9-N_{11}-C_{12}-H_{15}	-161.40	-173.95
O_{16}-N_{11}-C_{12}-H_{13}	-56.47	-74.04
O_{16}-N_{11}-C_{12}-H_{14}	-176.88	165.19
O_{16}-N_{11}-C_{12}-H_{15}	64.65	45.14
C_9-N_{11}-O_{16}-C_{17}	124.03	116.65
C_{12}-N_{11}-O_{16}-C_{17}	-100.47	-99.80
N_{11}-O_{16}-C_{17}-H_{18}	-61.01	-54.56
N_{11}-O_{16}-C_{17}-H_{19}	179.56	174.69
N_{11}-O_{16}-C_{17}-H_{20}	61.17	65.39

3.2. Vibrational Assignments

BMM has 25 atoms and it is a nonlinear molecule with 69 (3N-6) degrees of freedom vibrational modes, and the experimental bands corresponding to the 69 anticipated normal modes have been assigned using PED. Figs. 2 & 3 show an optical comparison of experimental and stimulated FT-IR and FT-Raman spectra. Vibrational assignments of BMM by Normal Coordinate Analysis based on SQMFF calculations and definition of local symmetry coordinates are shown in Tables 3 & 4. The experimental results are well-matched with the predicted theoretical values.

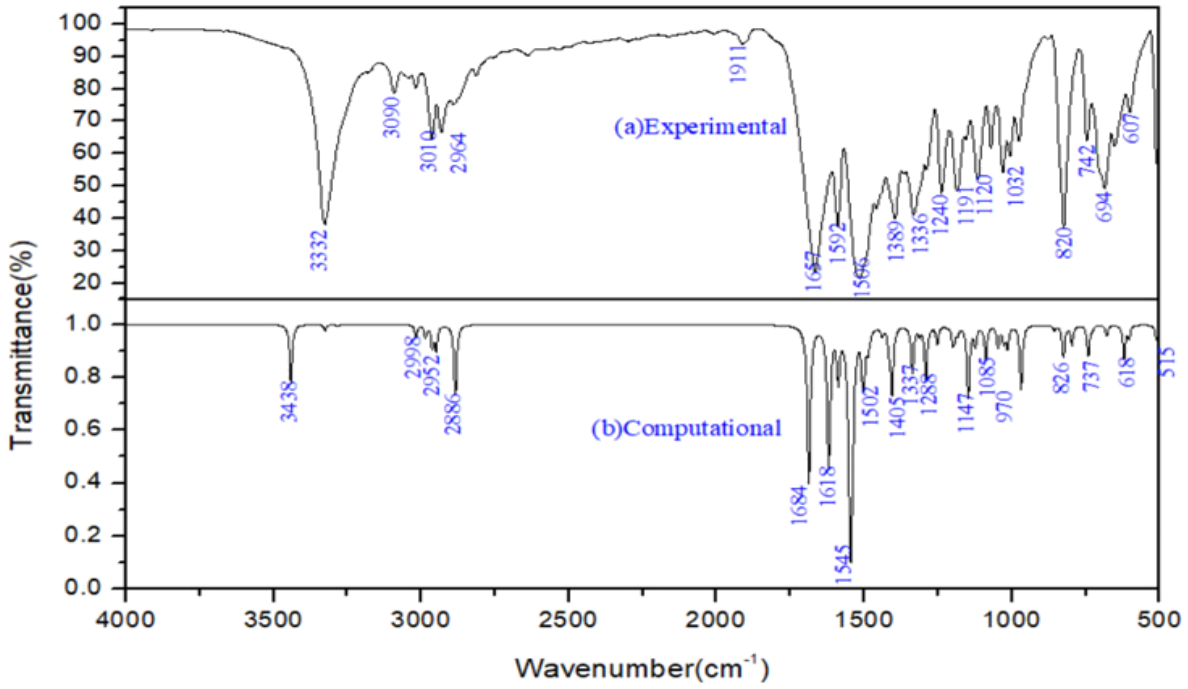


Fig. 2: Combined FT-IR (a) Experimental (b) Computational spectrum of BMM molecule

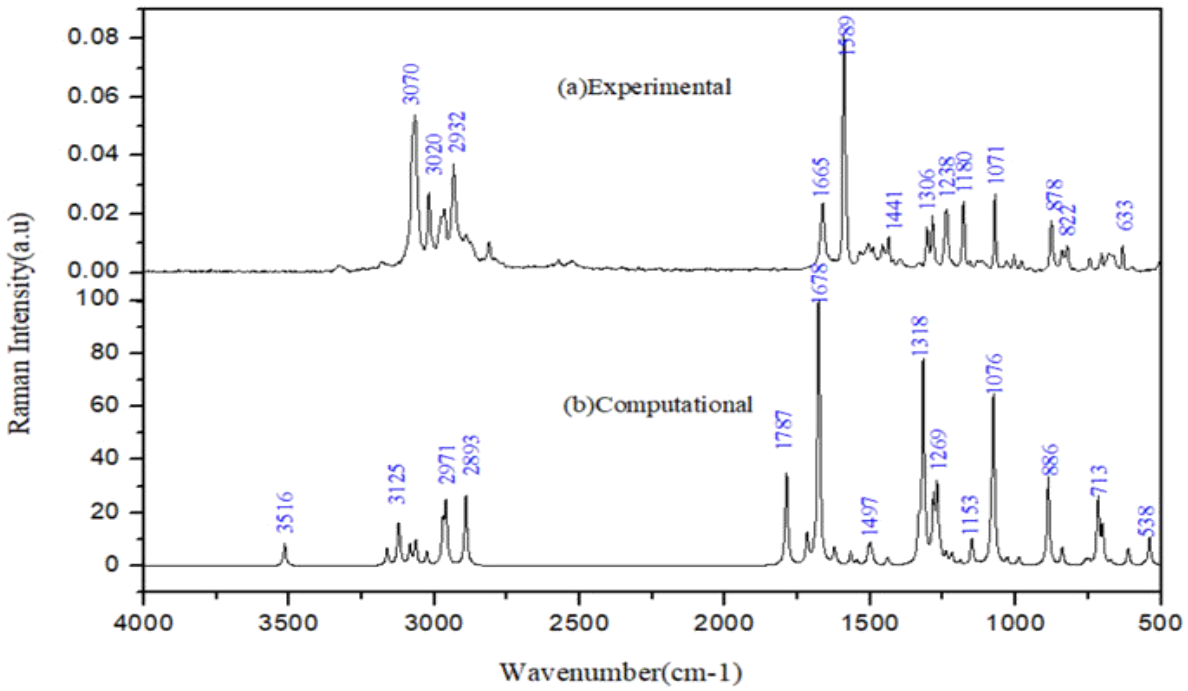


Fig. 3: Combined FT-Raman (a) Experimental (b) Computational spectrum of BMM molecule

3.2.1. Methoxy group ($O-CH_3$) and ($N-CH_3$) vibrations

The methoxy group vibrations play a significant function in the molecules stability [11]. The nine normal modes and twisting modes are related to the methoxy group vibrations. They are asymmetric stretching, symmetric stretching, in-plane stretching, out-of-plane stretching, symmetric bending, in-plane bending, out-of-plane bending, in-plane rocking and out-of-plane rocking [12]. Electronic processes alter the asymmetric and symmetric stretching modes of the methoxy group linked to the oxygen atom [13]. The C-H asymmetric stretching vibration of the $O-CH_3$ group occurs at $2970cm^{-1}$- $2920cm^{-1}$ [14]. The $O-CH_3$ asymmetric stretching mode has been ascribed to the FT-IR medium bands recorded at $2961cm^{-1}$(64 % PED) and $2927cm^{-1}$(62 % PED), as well as the FT-Raman strong and very strong bands observed at $2968cm^{-1}$(64 % PED) and $2934cm^{-1}$(62 % PED). This theoretical value shows good agreement with the experimental value. $N-CH_3$ absorbs in the $2805cm^{-1}$ to $2780cm^{-1}$ range due to its methyl symmetric stretch [15]. In this work, FT-IR weak band occurs at $2819cm^{-1}$ (66% PED) and FT-Raman medium band occurs at $2814cm^{-1}$ (66 % PED). The weak and medium FT-Raman bands observed at 1491 cm^{-1} (66% PED) and $1439cm^{-1}$(83% PED) have been assigned asymmetric and symmetric bending. The strong FT-IR band assigned at $1239cm^{-1}$ (73% PED) and $1189cm^{-1}$(29% PED). This shows the $N-CH_3$ group in-plane rocking and $O-CH_3$ group in out-of-plane rocking modes. The presence of hyper conjugate interaction is suggested by the huge FT-IR and FT-RAMAN wave number of the rocking mode [16].

3.2.2. C-H Vibrations

In general, the empirical value of C-H stretching vibration was $3100cm^{-1}$- $3000cm^{-1}$ [17]. In the BMM molecule, the C-H stretching vibration at $3323cm^{-1}$(very strong), $3096cm^{-1}$(weak) and $3020cm^{-1}$(weak) in FT-IR bands and $3186cm^{-1}$(very weak), $3069cm^{-1}$(very strong) and $3020cm^{-1}$(very strong) in FT-RAMAN bands were assigned with approximately 98% PED contribution. Weak bands for the BMM molecule may be seen in the above region, indicating that the carbon atoms were coupled to oxygen and nitrogen atoms. In strong FT-IR band observed at $1516cm^{-1}$(23% PED) indicates the C-H symmetric bending vibration mode. The very strong FT-RAMAN spectrum at $1179cm^{-1}$ is attributed to H-C-C bending.

3.2.3. C-C Vibrations

In Benzene, the stretching of C-C vibrations occur in the region $1200cm^{-1}$-$1650cm^{-1}$ [18]. FT-RAMAN spectrum bands are assigned at $1665cm^{-1}$(strong), $1287cm^{-1}$(strong) and $1240cm^{-1}$(very strong) and FT-IR bands are assigned at $1667cm^{-1}$(strong) and $1592cm^{-1}$(medium) respectively. Due to the components of other atoms, these bands give the ring C-C stretching vibration with low PED values. In the aforementioned area, the phenyl group's C-C stretching modes are expected. The form of replacement around the ring determines the actual placements of the modes [19].

3.2.4. C-Br Vibrations

The bonds between the ring and the halogen atoms play a crucial role in the vibrational assignment. Because of the reduction of molecular symmetry and the presence of heavy atoms, vibrations might mix. The vibrations are attributed C-X group (X= Cl, Br and I) in the frequency range of 1129-480 cm^{-1} [20]. The FT-IR spectrum band are occurs at $1067cm^{-1}$ in medium range, showing the C-Br stretching vibration. FT-RAMAN spectrum was assigned at $343cm^{-1}$ in the very strong band, giving wagging mode and symmetric bending with low PED value. The FT-RAMAN band observed at $95cm^{-1}$ very weak band, gives the Br-C-C symmetric bending.

3.2.5. Nitro group & O-C Vibrations

Because of the intra molecule charge transfer process, aromatic nitro compounds exhibit symmetric and asymmetric stretching vibrations [21]. The nitro compound bands are attributed in the region $1570cm^{-1}$-$1485cm^{-1}$ and $1370cm^{-1}$-$1320cm^{-1}$ for asymmetric and symmetric stretching vibrations respectively. In FT-IR spectrum band is observed at $827cm^{-1}$ (very strong) in symmetric N-O and N-C stretching vibration modes and C-O in-plane rocking modes. FT-Raman bands are observed at $120cm^{-1}$(very strong) and $95cm^{-1}$(very weak) for wagging and torsion modes of nitro groups respectively.

3.2.6. Force constant

The quantum mechanical computational analysis gives the output file, it is expressed the force constant in Cartesian coordinates. These force constants were translated into local symmetry coordinates using the MOLVIB software [22]. The potential energy distribution (PED) among the normal coordinates was calculated using local symmetry coordinates. Internal

local symmetry coordinates were used to compute the stretching force constants and tabulated in Table 4. The C-C, C-N stretching force constants have higher values, when comparing the C-H, C-Br stretching force constants [23]. The frequency of vibration is inversely proportional to the mass of the molecule and directly proportional to the force constant. Hence, the heavier molecules vibrate at lower frequencies.

Table 3: Vibrational assignments of BMM by Normal Coordinate Analysis based on SQMFF calculations

Observed fundamentals /cm^{-1}		Calculation	Intensity		Selective scaled B3LYP/6-311G++ (d,p) force field Assignment with PED (>10%)
υ_{IR}	υ_{Raman}	υ_{scal}	IR	RAMAN	
	3342 vw	3441	78.19	151.3	ν_s NH(99)
3323vs		3326	6.99	114.6	ν_s CH(98)
	3186 vw	3284	1.51	183.3	ν_s CH(99)
3096w	3069vs	3282	1.25	121.3	ν_s CH(98)
3020w	3020vs	3019	1.25	84.3	ν_s CH(98)
		3018	12.22	135.0	$\nu'_{as}CH_3(80)+\nu_{as}CH_3(13)$
		2986	14.65	163.4	$\nu_{as}CH_3(96)$
2961m	2968s	2963	27.99	210.6	$\nu_{as}CH_3(64)+\nu'_{as}CH_3(20)+\nu_sCH_3(15)$
2927m	2934vs	2949	30.50	84.9	$\nu'_{as}CH_3(99)$
	2887vw	2886	43.06	722.7	$\nu_sCH_3(62)+\nu_sCH_3(26)$
2819w	2814m	2884	56.49	81.1	$\nu_sCH_3(51)+\nu_sCH_3(33)+\nu_{as}CH_3(14)$
		1688	289.35	900.6	ν_s OC(66)+ βCNO(10)+ ν_s NC(10)
1667s	1665s	1621	32.41	3258.2	ν_s CC(30)
1592m		1588	103.70	51.6	ν_s CC(19)+ ρCN(14)+ ν_s CC(12)+ ν_s CC(11)
		1546	792.13	982.2	ρCN(22)+ ν_s NC(17)+ ν_s CN(11)
1516s		1505	80.05	106.7	βHCC(23)+ βHCC(19)+ ν_s CC(11)
		1499	9.29	139.7	$\delta CH_3(69)$
		1489	10.14	99.4	$\gamma CH_3(37)+\gamma CH_3(37)$
	1491w	1486	30.38	131.4	$\delta CH_3(66)+$ ρCO(10)
		1481	3.04	92.0	$\gamma CH_3(45)+\gamma CH_3(27)$
	1439m	1439	11.50	61.4	$\beta CH_3(83)$
		1415	28.15	47.2	$\beta CH_3(67)$
1399s		1406	87.79	122.4	$\beta CH_3(15)+$ βHCC(15)+ ν_s CC(14)+ ν_s CC(12)+ βHCC(11)
1335s		1337	113.17	413.9	βHCC(27)+ βHCC(22)
		1314	15.20	612.6	ν_s NC(25)+ ν_s CN(24)
	1287s	1292	31.37	583.4	ν_s CC(19)+ ν_s CC(16)+ ρCN (10)
	1240vs	1253	78.84	1253.5	ν_s CC(20) + ν_s CC(13) + ν_sCC(11)+ ν_sCC(10)
1239s		1221	1.36	46.4	$\rho CH_3(73)$
1189s		1201	3.25	972.1	$\rho' CH_3(29)$
	1179vs	1196	57.36	83.9	βHCC(15)+ βHCC(15)+ βHCC(14)+ βHCC(14)
		1185	9.68	117.2	$\rho' CH_3(90)$
		1148	15.82	59.2	$\rho CH_3(57)+\nu_s$ NC(11)
1118m		1124	84.26	80.0	ν_s CC(18)+ ν_s CC(18)+ βHCC(14)+ βHCC(13)+ βHCC(12)+ βHCC(11)
	1071vs	1089	48.56	398.7	ν_s NC(41)+ ν_s NO(14)
1067m		1047	34.85	1256.0	ν_s CC(27)+ ν_s CC(25)+ ν_s CBr(14)

		1029	59.61	97.1	δring(68)+ v_s CC(12)
	1005w	1016	25.10	422.2	v_s OC(29)+ v_s NC(10)+ ρ'CH_3 v_s NO(21)+ (10)
978w		969	18.34	64.5	v_s OC(54)
		951	52.94	107.3	ωCH(48)+ ωCH(33)
883vw		910	0.12	16.7	ωCH(43)+ ωCH(30)+ Puck(ring)(15)
	878s	857	4.15	1211.6	βCNH(19)+ v_s CC(18)
827vs		829	38.50	22.6	v_s NO(16)+ v_s NC(16)+ ρCO(15)
	824m	826	14.15	128.0	ωCH(46)+ ωCH(32)
		796	23.41	15.3	ωCH(48)+ ωCH(27) +ωCH(10)
746m	745m	743	36.88	97.1	ωOCN(79)
		729	4.73	109.2	Puck(ring)(70)+ ωCH(11)
688s		680	13.14	1538.4	γ ring(38)+ v_s CBr(11)
651w		655	0.12	470.2	$\gamma_a$ring(77)
	629m	619	45.76	98.0	τCN(29)+ ωHNC(24)
602w		602	12.14	166.5	ωCH(18)+ ρCO(14)+ v_s NO(13)+ ωHNC(10)
508s	511w	512	16.78	72.8	τ ring(36)+ ωNC(33)+ ωCH(18)
		484	4.90	865.1	ρCO(37)+ βNCO(17)
464m		446	28.45	1167.8	ωCH(39)+ ρCO(20)+ ωONC(16)
413s		435	0.05	16.2	$\tau_a$ring(83)
	394vw	391	27.01	334.1	βNCC(29)+ ρCO(21)+ βCNH(15)
		373	1.13	217.7	βCNO(34)+ ρCO(19)+ v_s CBr(10)
	343vs	331	19.27	522.9	βCNO(15)+ ωBrC (14)+ βBrCC(11) +βNCC(10)
	307vw	319	5.36	693.8	ωCH(29)+ τ ring(16)
		233	8.63	244.7	ωONC(34)+ ωCH(10)
		224	1.08	2251.8	βBrCC(39)+ βCNH(12)+ v_sCBr(10)
		194	1.08	970.3	τOC(37)+ ωONC(21)
		172	1.16	1050.4	τNC(57)+ τOC(17)
		170	0.37	2368.6	τNC(26)+ τOC(22)+ ωONC(12)
	120vs	137	0.68	3156.2	ωHNC(21)+ ωBrC(16)+ $\tau_a$ring(16)+ τCN(15)
	95vw	99	1.22	2918.5	τNO(27)+ βCNH(13)+ βNCC(11)+ τCN(11)+ βBrCC(10)
		87	4.49	768.1	τCN(58)
		71	2.70	7183.4	τNO(55)+ τCN(11)
		34	0.09	63309.7	τCN(52)+ ωHNC(27)
		32	0.62	55756.9	τCN(29)+ τCN(18)+ τNO(12)

vs: very strong; s: strong; w: weak; vw: very weak; v_s: symmetric stretching; v_{as}: asymmetric stretching; β: symmetric bending; γ: in-plane bending; γ_a: out-of-plane bending; δ: asymmetric bending; ρ: in-plane rocking; ρ': out-of-plane rocking; puck: puckering; ω: wagging; τ: torsion

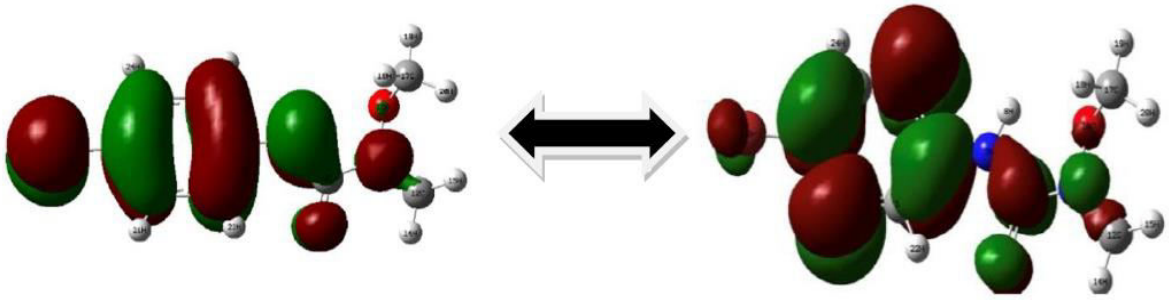
3.3. Frontier Molecular Orbital Analysis

Frontier molecular orbitals, such as HOMO and LUMO, are critical in the kinetic stability and chemical reactivity of any substance [24]. The orbitals at the molecules outermost surface from where electron delocalization can occur are referred to as the frontier [25]. The HOMO and LUMO are more than the complete molecule excluding two methyl groups. This indicates the HOMO-LUMO is maximum localized in the anti bonding type orbitals. The energy values of the FMO can be used to calculate some motivating reactivity indices for the compound. The bandgap energy of the BMM molecule is E_{HOMO}=6.2134eV, E_{LUMO}=0.8359ev, Energy gap=5.3775ev. Fig 4 shows the HOMO and LUMO of BMM molecule.

Table 4: Definition of local symmetry coordinates

No	Symbol	Definition	Scale factor	Force constant (mdyne/A°)
Stretching				
1-6	ν_s (CC)	R_1,R_2,R_3,R_4,R_5,R_6	0.91294	0.021
7-10	ν_s (CH)	r_7,r_8,r_9,r_{10}	1.05412	0.0764
11	ν_s (CBr)	r_{11}	0.91073	0.1041
12	ν_s (CN)	r_{12}	1.05412	0.3385
13	ν_s (NH)	r_{13}	0.91294	0.3304
14	ν_s (NC_1)	r_{14}	1.05412	0.3599
15	ν_s (NC_2)	r_{15}	1.05412	0.6002
16	ν_s (NC_3)	r_{16}	0.91073	0.3160
17	ν_s (NO)	r_{17}	0.91073	0.4538
18-19	ν_s (OC)	r_{18},r_{19}	0.91073	0.7173
20	$\nu_s(CH_3)$	$(r_{20}+r_{21}+r_{22})/\sqrt{3}$	0.91173	0.8314
21	$\nu_{as}(CH_3)$	$(2r_{20}-r_{21}-r_{22})/\sqrt{6}$	0.91173	0.2838
22	$\nu'_{as}(CH_3)$	$(r_{21}-r_{22})/\sqrt{2}$	0.91073	1.7350
23	$\nu_s(CH_3)$	$(r_{23}+r_{24}+r_{25})/\sqrt{3}$	0.91173	1.5035
24	$\nu_{as}(CH_3)$	$(2r_{23}-r_{24}-r_{25})/\sqrt{6}$	0.91173	1.0598
25	$\nu'_{as}(CH_3)$	$(r_{24}-r_{25})/\sqrt{2}$	0.91173	3.6595
Bending				
26-29	β(HCC)	$(\beta_{26}-\beta_{27})/\sqrt{2},(\beta_{28}-\beta_{29})/\sqrt{2},(\beta_{30}-\beta_{31})/\sqrt{2},(\beta_{32}-\beta_{33})/\sqrt{2}$	1.00722	1.3450
30	β(NCC)	$(\beta_{34}-\beta_{35})/\sqrt{2}$	1.04555	0.6930
31	β(BrCC)	$(\beta_{36}-\beta_{37})/\sqrt{2}$	1.02844	1.5155
32	δ(ring)	$(\delta_{37}-\delta_{38}+\delta_{39}-\delta_{40}+\delta_{41}-\delta_{42})/\sqrt{6}$	1.04555	0.8853
33	γ (ring)	$(2\delta_{37}-\delta_{38}-\delta_{39}+2\delta_{40}-\delta_{41}-\delta_{42})/\sqrt{6}$	1.04555	2.7749
34	γ_a(ring)	$(\delta_{38}-\delta_{39}+\delta_{41}-\delta_{42})/2$	1.04555	3.3725
35	β(NCO)	$(2\beta_{43}-\beta_{44}-\beta_{45})/\sqrt{6}$	0.91073	1.8837
36	ρ(C-O)	$(\beta_{44}-\beta_{45})/\sqrt{2}$	1.04555	2.5151
37	$\beta(CH_3)$	$(\alpha_{46}+\alpha_{47}+\alpha_{48}-\beta_{49}-\beta_{50}-\beta_{51})/\sqrt{6}$	0.97048	1.2174
38	$\delta(CH_3)$	$(2\alpha_{46}-\alpha_{47}-\alpha_{48})/\sqrt{6}$	0.97048	1.1222
39	$\gamma(CH_3)$	$(\alpha_{47}-\alpha_{48})/\sqrt{2}$	1.00722	1.0317
40	$\rho(CH_3)$	$(2\beta_{49}-\beta_{50}-\beta_{51})/\sqrt{6}$	1.02844	1.5987
41	$\rho'(CH_3)$	$(\beta_{50}-\beta_{51})/\sqrt{2}$	1.02844	0.9911
42	$\beta(CH_3)$	$(\alpha_{52}+\alpha_{53}+\alpha_{54}-\beta_{55}-\beta_{56}-\beta_{57})/\sqrt{6}$	0.97048	1.3089
43	$\delta(CH_3)$	$(2\alpha_{52}-\alpha_{53}-\alpha_{54})/\sqrt{6}$	1.00722	2.1123
44	$\gamma(CH_3)$	$(\alpha_{53}-\alpha_{54})/\sqrt{2}$	0.97048	3.6871
45	$\rho(CH_3)$	$(2\beta_{55}-\beta_{56}-\beta_{57})/\sqrt{6}$	1.02844	2.7879
46	$\rho'(CH_3)$	$(\beta_{56}-\beta_{57})/\sqrt{2}$	1.02844	2.1057
47	β(CNH)	$(2\beta_{58}-\beta_{59}-\beta_{60})/\sqrt{6}$	1.04555	2.8918
48	ρ(C-N)	$(\beta_{59}-\beta_{60})/\sqrt{2}$	0.97048	1.5253
49	β(CNO)	$(2\beta_{61}-\beta_{62}-\beta_{63})/\sqrt{6}$	1.02844	1.4305
50	ρ(C-O)	$(\beta_{62}-\beta_{63})/\sqrt{2}$	0.91073	1.3538
51	β(NOC)	β_{64}	1.04555	1.3656

Wagging				
52-55	ω(C-H)	$\omega_{65}, \omega_{66}, \omega_{67}, \omega_{68}$	0.94869	2.3120
56	ω(N-C)	ω_{69}	0.97048	7.0387
57	ω(Br-C)	ω_{70}	0.94869	8.8087
58	ω(OCN)	ω_{71}	0.97048	17.8190
59	ω(HNC)	ω_{72}	0.89628	5.5835
60	ω(ONC)	ω_{73}	1.06042	5.5736
Torsion				
61	Puck(ring)	$(\tau_{74}- \tau_{75}+ \tau_{76}- \tau_{77}+ \tau_{78}- \tau_{79})/ \sqrt{6}$	1.06042	6.2343
62	τ(ring)	$(\tau_{75}- \tau_{77}- \tau_{76}- \tau_{79})/2$	1.06042	6.2095
63	τ_a(ring)	$(-\tau_{74}+2\tau_{75}- \tau_{76}- \tau_{77}+ 2\tau_{78}- \tau_{79})/ \sqrt{12}$	1.06042	6.3620
64	τ(CN)	$(\tau_{80}+\tau_{81}+ \tau_{82}+ \tau_{83})/2$	0.89628	6.4084
65	τ(CN)	$(\tau_{84}+\tau_{85}+\tau_{86}+ \tau_{87})/2$	0.89628	6.4740
66	τ(CN)	$(\tau_{88}+\tau_{89+}\tau_{90}+\tau_{91})/2$	1.06042	6.5730
67	τ(NO)	$(\tau_{92}+\tau_{93})/ \sqrt{2}$	0.89628	6.6011
68	τ(OC)	$(\tau_{94}+\tau_{95}+ \tau_{96})/ \sqrt{3}$	0.89628	6.7584
69	τ(NC)	$(\tau_{97}+\tau_{98}+ \tau_{99}+\tau_{100}+ \tau_{101}+\tau_{102})/ \sqrt{6}$	0.89628	8.2192



HOMO **LUMO**

Fig. 4: HOMO -LUMO of the BMM molecule

3.4. Global Reactivity Descriptors

Using Koopmans's theorem for the BMM molecule, global reactivity descriptors were calculated, That is,

Ionization Energy (I) $=-E_{HOMO}$,

Electron Affinity (A) $=-E_{LUMO}$,

Chemical Hardness (η) = (I-A)/2,

Chemical Potential (μ) = - (I+A)/2

Electro negativity (χ) = (I+A)/2,

Chemical Softness (τ) = 1/ (2η),

Electrophilicity index (ω) = $\mu^2/2\eta$ [26].

The values of the Electrophilicity index of the BMM molecule propose the biological activity. The molecules electrophilic power is a measurement of how much energy is lost due to maximum electron movement between donor and acceptor [27]. Chemical hardness is high, and molecular charge transfer is low. Hard molecules, on the other hand, have a big energy gap while soft molecules have a tiny energy gap. As a result, rigid molecules are less polarizable than softness [28]. Aromatic compounds anticorrosive abilities are based on their ability to react on metal surfaces when water molecules are replaced [29]. The place of corrosion can be linked to EHOMO, after which the donor orbital interacts with the inhibitors -electrons, resulting in inhibition efficiency [30]. The bandgap measurements of BMM molecules demonstrate that they have a high EHOMO and a low ELUMO. The global reactivity descriptors values are reported in Table 5. The corrosion inhibition efficiency, polarizability, kinetic stability, and chemical reactivity of the BMM molecule are all high. As a result, it can be employed in both industrial and pharmaceutical settings.

Table 5: Global reactivity descriptors values based on HOMO-LUMO of BMM molecule

Ionization energy(I)	6.2134 [eV]
Electron affinity(A)	0.8359 [eV]
Chemical Hardness(η)	2.6888 [eV]
Electro negativity(χ)	3.5247 [eV]
Chemical Potential(μ)	-3.5247 [eV]
Chemical Softness(τ)	0.1860 [eV^{-1}]
Electrophilicity index (ω)	2.3102 [eV]

3.5. MEP analysis for Reactivity

MEP refers to a molecule's overall reactivity towards similar nucleophiles and electrophiles. It determines the charge domains of the molecule and predicts its biological activity. The red portions are more electronegative, attracting electrophiles, whereas the blue portions are more electropositive, attracting more nucleophiles [31]. The general color code is red<orange<yellow<green<blue [32]. The green regions are represents the zero potential. The electrostatic potential is negative in locations where electrons are abundant (O_{10}, O_{16}, Br_{25}). The electrostatic potential is positive in areas where electrons are scarce (remaining more molecules). The binding energy between the receptor and substrate sites electrostatic potential values can be utilized. Molecular potential mapped on the isodensity surface in the range from -0.05048(red) to +0.05048(blue) for calculated at the B3LYP/6-311++G (d, p) basis set. Fig. 5 shows MEP diagram of the BMM molecule. The active areas sites are evidence of the BMM compounds biological activity and chemical processes, which led to its use in the field of biochemistry.

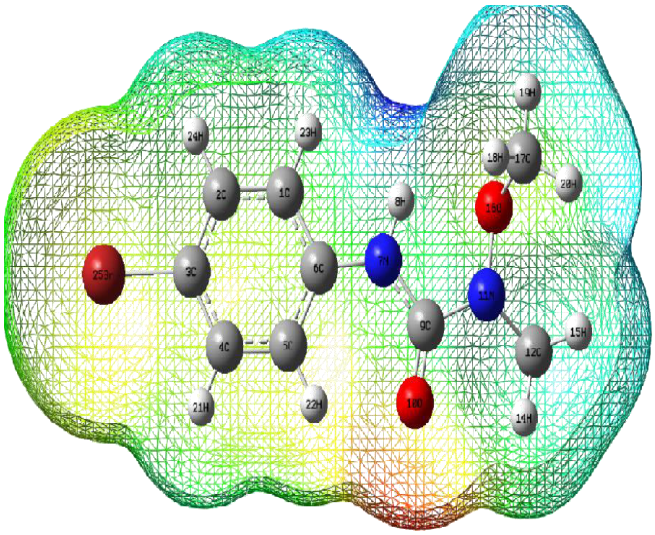


Fig. 5: MEP of BMM molecule

3.6. UV Analysis

The Beer-Lambert equation is used to determine the relationship between absorption and concentration. If the excitation of the outermost electrons is high, the absorption is high. UV rays have enough energy to excite electrons in their outermost states to higher energy levels [33]. The UV spectral analysis of the BMM molecule was explored using the TD-DFT/B3LYP/6-311++G (d, p) level basis set and methanol is used as the solvent. The TD-DFT method measures the transition properties of the compound in their higher states. In a methanol solvent, the computed findings for vertical excitation energies, oscillator strength (f), absorption wavelength, and significant contributions were performed and tabulated (Table 6).

Table 6: Calculated absorption wavelength, energies, Oscillator strengths and major contributions of BMM using the TD-DFT method in methanol solvent

NO	Band gap Energy [eV]		Wavelength[nm]		Oscillator strength(f)	Symmetry	Major contributions
	Theo.	Exp.	Theo.	Exp.			
1.	4.6805		264.89		0.0191	Singlet-A	H-2->LUMO (11%), HOMO->L+1 (79%)
2.	4.8476		255.76		0.0125	Singlet-A	HOMO->L+2 (94%)
3.	5.1057	5.1622	243.73	245	0.7015	Singlet-A	HOMO->LUMO(85%)
4.	5.5726		222.48		0.0056	Singlet-A	HOMO->L+3 (94%)
5.	5.7014		217.46		0.0099	Singlet-A	H-3->LUMO (22%), H-1->LUMO (56%)
6.	5.7897		214.14		0.0039	Singlet-A	H-1->LUMO (10%), H-1->L+1 (82%) H-2->LUMO (4%)

The maximum absorption peak (max) in the UV-Vis spectrum predicts an electronic transition as a very strong band at 243 nm with an oscillator strength of f=0.7015, which is observed at 245 nm and is designated as $\pi \rightarrow \pi^*$ transition. The wavelength of HOMO-LUMO is 269 nm. There is good agreement when comparing the UV-Vis theoretical and UV-Vis experimental. Electron delocalization from the HOMO to LUMO+2 and HOMO to LUMO+3 orbitals contributed 94 percent and HOMO to LUMO orbitals contributed 85 percent to electron localization. Theoretically, these assignments have been seen.

3.7. NBO Analysis

The NBO analysis is the process of converting multi-electron wave functions of molecules into single-centered (lone pair (n1, n2, n3)) and two-centered (natural bond and antibonding orbitals (BD (1), BD (2), BD* (1) and BD* (2)) components. It calculates the intramolecular and intermolecular orbital interactions in molecules containing filled donor and empty acceptor NBOs, allowing us to make a quantitative assessment [34]. Charge transfer from the highest occupied bonding orbital into an unoccupied antibonding orbital can cause delocalization effects. The energy lowering interaction is given by the second-order perturbation [35]. Table 7 shows the results of a second order perturbation theory study of the fock matrix NBO basis.

The more donating tendency of electron donors have the greater level of conjugation of the compounds, so the E (2) value is larger [36]. The B3LYP/6-311++G (d, p) level NBO analysis was done on the BMM molecule to explain the delocalization of electron density within the molecule. The presence of N-C…O and C-N…O intramolecular contacts between the p-type lone pair of the n2 (O_{10}) and the sequestered $\sigma^*(N_7\text{-}C_9)$ and $\sigma^*(C_9\text{-}N_{11})$ anti-bonds is shown by the hyper conjugative interactions of the p-type lone pair of the n2 (O_{10}) with the secluded $\sigma^*(N_7\text{-}C_9)$ and $\sigma^*(C_9\text{-}N_{11})$ anti-bond.

Table 7: Second order perturbation theory Analysis of Fock Matrix NBO basis

Donor NBO(i)	E.D (i)(e)	Acceptor NBO(j)	E.D(j)(e)	$E^{(2)}$ [kcal/mol]	E(j)-E(i) [a.u]	F(i,j) [a.u]
σ (C_1-C_2)	1.96752	σ^* (C_3-Br_{25})	0.03585	5.53	0.80	0.060
π(C_1-C_2)	1.70215	π^*(C_3-C_4)	0.39467	17.69	0.28	0.064
π(C_1-C_2)	1.70215	π^*(C_5-C_6)	0.38095	19.97	0.29	0.069
π(C_3-C_4)	1.68799	π^*(C_1-C_2)	0.33677	21.47	0.29	0.071
π(C_3-C_4)	1.68799	π^*(C_5-C_6)	0.38095	16.92	0.29	0.064
σ(C_4-C_5)	1.96683	σ^*(C_3-Br_{25})	0.03585	5.61	0.79	0.060
π(C_5-C_6)	1.62988	π^* (C_1-C_2)	0.33677	19.09	0.28	0.066
π(C_5-C_6)	1.62988	π^*(C_3-C_4)	0.39467	23.33	0.27	0.072
n1(N_7)	1.68406	π^* (C_5-C_6)	0.38095	34.18	0.30	0.091
n1(N_7)	1.68406	σ^*(C_9-O_{10})	0.17866	13.98	0.60	0.085
n1(N_7)	1.68406	π^* (C_9-O_{10})	0.21206	13.30	0.54	0.078
n2(O_{10})	1.84179	σ^*(N_7-C_9)	0.07196	23.32	0.70	0.116
n2(O_{10})	1.84179	σ^*(C_9-N_{11})	0.08737	25.70	0.64	0.116
n1(N_{11})	1.81486	σ^*(C_9-O_{10})	0.17866	7.89	0.66	0.065
n1(N_{11})	1.81486	π^* (C_9-O_{10})	0.21206	10.49	0.59	0.071
n1(N_{11})	1.81486	σ^*(C_{12}-H_{13})	0.01689	5.77	0.71	0.060
n2(O_{16})	1.94059	σ^*(N_7-H_8)	0.02362	2.19	0.74	0.036
n2(O_{16})	1.94059	σ^*(C_9-N_{11})	0.08737	2.71	0.73	0.040
n2(O_{16})	1.94059	σ^*(N_{11}-C_{12})	0.01670	3.68	0.67	0.045
n2(O_{16})	1.94059	σ^*(C_{17}-H_{18})	0.01620	4.66	0.72	0.052
n2(O_{16})	1.94059	σ^*(C_{17}-H_{20})	0.01639	5.54	0.72	0.057
n2(Br_{25})	1.97667	σ^*(C_2-C_3)	0.02613	3.26	0.86	0.047
n2(Br_{25})	1.97667	σ^*(C_3-C_4)	0.02617	3.23	0.86	0.047
n3(Br_{25})	1.94306	π^*(C_3-C_4)	0.39467	9.19	0.31	0.052

The resonance of the asymmetric phenyl ring is amplified by electron donating oxygen atom due to the lengthening of C-O and N-O bonds. The existence of C-C…N, C-O…N, and C-O…N intramolecular

contacts is shown by the lone pair of the n1 (N_7) with the remote π* (C_5-C_6), σ*(C_9-O_{10}) and π* (C_9-O_{10}) anti-bonds, whose energy contributions are 34.18 kJ/mol, 13.98 kJ/mol, and 13.30 kJ/mol, respectively. The π* (C_9-O_{10}) NBO will further transfer its electrons to σ*(C_9-O_{10}) orbital with the higher hyper conjugation of 318.79 kJ/mol. The intramolecular $E^{(2)}$ interaction energy is formed by the orbital overlap between π(C-C) and π *(C-C) anti-bond orbitals which results in intramolecular charge transfer ICT causing stabilization of the system. The π (C_1-C_2) and π (C_3-C_4) bonds transfers to π *(C_3-C_4), π *(C_5-C_6) and π* (C_1-C_2), π*(C_5-C_6) anti-bond orbitals with $E^{(2)}$ interaction energy 17.69 kJ/mol, 19.97 kJ/mol and 21.47 kJ/mol, 16.92 kJ/mol respectively. These interactions are observed as an increase in electron density ED in C-C anti-bonding orbital that weakens the respective bonds [37]. The zero-point vibrational energy is 121.4079kcal/mol in the molecule. The natural population core is 53.9889 and valence is 75.7072. Natural minimal Basis and Natural Ryberg Basis are 129.6961 and 0.30389. The intramolecular charge transfer is one of the causes of the biological activity of the BMM molecule.

3.8. Fukui function

To illustrate chemical reactivity and selectivity, the Fukui function is used as the local reactivity descriptor. It reveals the relative energy site in the molecule [38]. The Fukui functions are derived from the Hirshfeld partitioning of the electron density of neutral atoms (N), anionic (N+1), and cationic (N1) species, and provide more site selectivity and qualitative reactivity descriptors within the molecule. The condensed form of Fukui functions such as f_r°, f_r^+, and f_r^- for the radical, nucleophilic, and electrophilic attack on an atom of a molecule, respectively [39]. It can be expressed as

$f_r^\circ = 1/2[q_{(N-1)} - q_{(N+1)}]$.....(1a)

$f_r^+ = [q_{(N)} - q_{(N+1)}]$ .....(1b)

$f_r^- = [q_{(N-1)} - q_{(N)}]$ .....(1c)

Table 8 summarizes the calculated Fukui functions as well as the relative electrophilicity and nucleophilicity indices. Under this study, the relative electrophilicity (fr^+/fr^-) and corresponding nucleophilicity (fr^-/fr^+) are calculated [40]. This clearly shows the BMM molecule's more electrophilic attack and biological activity.

Table 8: Condensed Fukui function f_r for BMM molecule

Atom	Natural atomic charges(q)			Fukui functions				
	N (0,1)	N+1 (-1,2)	N-1 (1,2)	f_r^+	f_r^-	f_r^0	f_r^+ / f_r^-	f_r^- / f_r^+
C1	-0.2165	-0.2297	-0.0335	0.0135	0.1830	0.0983	0.0738	13.5463
C2	-0.2132	-0.2237	-0.1025	0.0105	0.1107	0.0606	0.0947	10.5640
C3	-0.1207	-0.1453	0.0900	0.0246	0.2107	0.1177	0.1167	8.5702
C4	-0.2054	-0.2197	-0.1010	0.0145	0.1044	0.0594	0.1389	7.1993
C5	-0.2161	-0.2236	-0.0331	0.0075	0.1830	0.0953	0.0411	24.3041
C6	0.1617	0.1561	0.1784	0.0056	0.0168	0.0112	0.3343	2.9910
N7	-0.6220	-0.6234	-0.1303	0.0014	0.4917	0.2465	0.0029	348.7376
H8	0.4121	0.3714	0.2140	0.0407	-0.1981	-0.0787	-0.2054	-4.8683
C9	0.8095	0.8027	0.3825	0.0068	-0.4270	-0.2101	-0.0159	-62.6026
O10	-0.6419	-0.6660	-0.2915	0.0241	0.3504	0.1872	0.0687	14.5378
N11	-0.2324	-0.2319	-0.0189	-0.0006	0.2136	0.1065	-0.0026	-381.393
C12	-0.3688	-0.3800	-0.1891	0.0112	0.1797	0.0954	0.0620	16.1166
H13	0.1883	0.1517	0.1124	0.0366	-0.0759	-0.0197	-0.4822	-2.0738
H14	0.2341	0.2052	0.1221	0.0289	-0.1120	-0.0416	-0.2581	-3.8741
H15	0.1925	0.1267	0.1099	0.0658	-0.0826	-0.0084	-0.7961	-1.256
O16	-0.4529	-0.4586	-0.2147	0.0057	0.2382	0.1219	0.0238	42.0883
C17	-0.1961	-0.2387	-0.1017	0.0426	0.0944	0.0685	0.4512	2.2161
H18	0.1744	0.0839	0.0886	0.0906	-0.0858	0.0024	-1.0551	-0.9478
H19	0.1873	-0.0049	0.1027	0.1922	-0.0846	0.0538	-2.2718	-0.4402
H20	0.1720	0.0455	0.0941	0.1265	-0.0779	0.0243	-1.6244	-0.6156
H21	0.2217	0.2073	0.1261	0.0144	-0.0956	-0.0406	-0.1507	-6.6368
H22	0.2513	0.2426	0.1361	0.0088	-0.1152	-0.0532	-0.0760	-13.153
H23	0.2038	0.0736	0.1148	0.1302	-0.089	0.0206	-1.4631	-0.6835
H24	0.2214	0.1911	0.1261	0.0304	-0.0954	-0.0325	-0.3186	-3.1392
Br25	0.0559	-0.0120	0.2183	0.0679	0.1625	0.1152	0.4178	2.3932

3.9. NLO analysis

The dipole moment during electron delocalization from HOMO to LUMO orbitals is explained by the electronic properties of BMM. The charge transfer between orbitals can explain NLO properties. Organic materials have been used as optoelectronic devices for telecommunication, optical data storage, sensor and solar cell fabrication, and so on in recent decades by computing the quantum mechanical effect of radiation on organic molecules [41]. The NLO properties of the BMM molecule have also been investigated using a DFT/ B3LYP/6-311++G (d, p) level basis set with the uptake of dipole moment(μ), polarizability (α), hyper polarizability (β) and second order hyperpolarizability (γ) are tabulated in Table 9. This tabulation shows the β and μ values indicating the industrial application of NLO material. The calculated first-order hyper-polarizability of the BMM molecule is $44.19x10^{-23}$ e.s.u., which is greater than that of the urea fragment. Hence it indicates NLO activity. The high polarizability shows the charge delocalization within the molecule.

Table 9: The values of calculated dipole moment μ(D), polarizability (α), first order hyperpolarizability (β) and second order hyperpolarizability (γ) components of BMM molecules

Parameter	B3LYP/6-311++G(d, p)	Parameter	B3LYP/6-311++G(d, p)	Parameter	B3LYP/6-311++G(d, p)
μ_x	4.20	β_{xxx}	45.10	γ_{xxxx}	-5797.19
μ_y	3.19	β_{xxy}	17.32	γ_{xxxz}	52.63
μ_z	0.12	β_{xyy}	-31.04	γ_{zzzy}	4.23
μ[D]	5.28	β_{yyy}	23.42	γ_{xxyz}	49.77
α_{xx}	-83.27	β_{xxz}	10.38	γ_{yyyy}	-747.80
α_{xy}	7.90	β_{xyz}	15.28	γ_{yyyx}	69.02
α_{yy}	-92.15	β_{yyz}	0.11	γ_{xxyy}	-1130.00
α_{xz}	1.59	β_{xzz}	-28.51	γ_{yyxz}	4.60
α_{yz}	0.89	β_{yzz}	-0.36	γ_{zzzz}	-179.11
α_{zz}	-98.69	β_{zzz}	0.16	γ_{yyyz}	-9.91
α[e.s.u]	$-91.37x10^{-23}$	β_{tot}[e.s.u]	$44.19x10^{-23}$	γ_{xxzz}	-1129.09
				γ_{zzxy}	1.44
				γ_{xxxy}	51.98
				γ_{zzzx}	-8.65
				γ_{yyzz}	-162.32

3.10. Molecular Docking

Molecular docking can be used to study the atomic interactions between ligands and proteins [42]. The protein 3D structure was obtained from the Protein Data Bank of the Research Collaboratory for Structural Bioinformatics (RCSB). The target proteins PDB IDs are 1UZY, 4MY1, and 5HCG. All water molecules have been removed, and short chains and polar hydrogen atoms have been added using Auto Dock 4.2.6, Auto Grid4.0 software, and the Kollman-Gasteiger atomic charge estimation scheme [43]. The proteins are then prepared and saved in PDBQT format. The BMM molecule is in sdf file format and was obtained from the Pubchem database. The ligand has been assigned Kollman-Gasteiger charges, which are saved in the PDBQT format [44]. Table 10 shows the bonded residues, bond binding energies, and intermolecular energies. Non-covalent interactions allow BMM to bind at the active site of the given proteins. The minimum binding energy of 5HCG protein is -4.97, indicating that the compound is stable. As a result, BMM has been well docked in the sites of 1UZY, 4MY1, and 5HCG. So BMM may be used in pharmaceutical applications, particularly as a hydrolyze enzyme inhibitor to treat cancer and other diseases. Pymol viewer is being used to visualize the interaction between the proteins and the ligands (Fig. 6). The maximum binding affinity in protein 4MY1 was pragmatic, with a binding energy of 6.46 kcal /mol and a hydrogen bond interaction at the position SER306, GLY364. The BMM compound binds

to the protein 1UZY with a binding energy of 5.36 kcal/mol and forms hydrogen bonds with the residues ASP89, GLY107, and ASN133. With a binding affinity of 4.97 kcal/ mol, the protein 5HCG forms a hydrogen bond interaction at position TRP232.

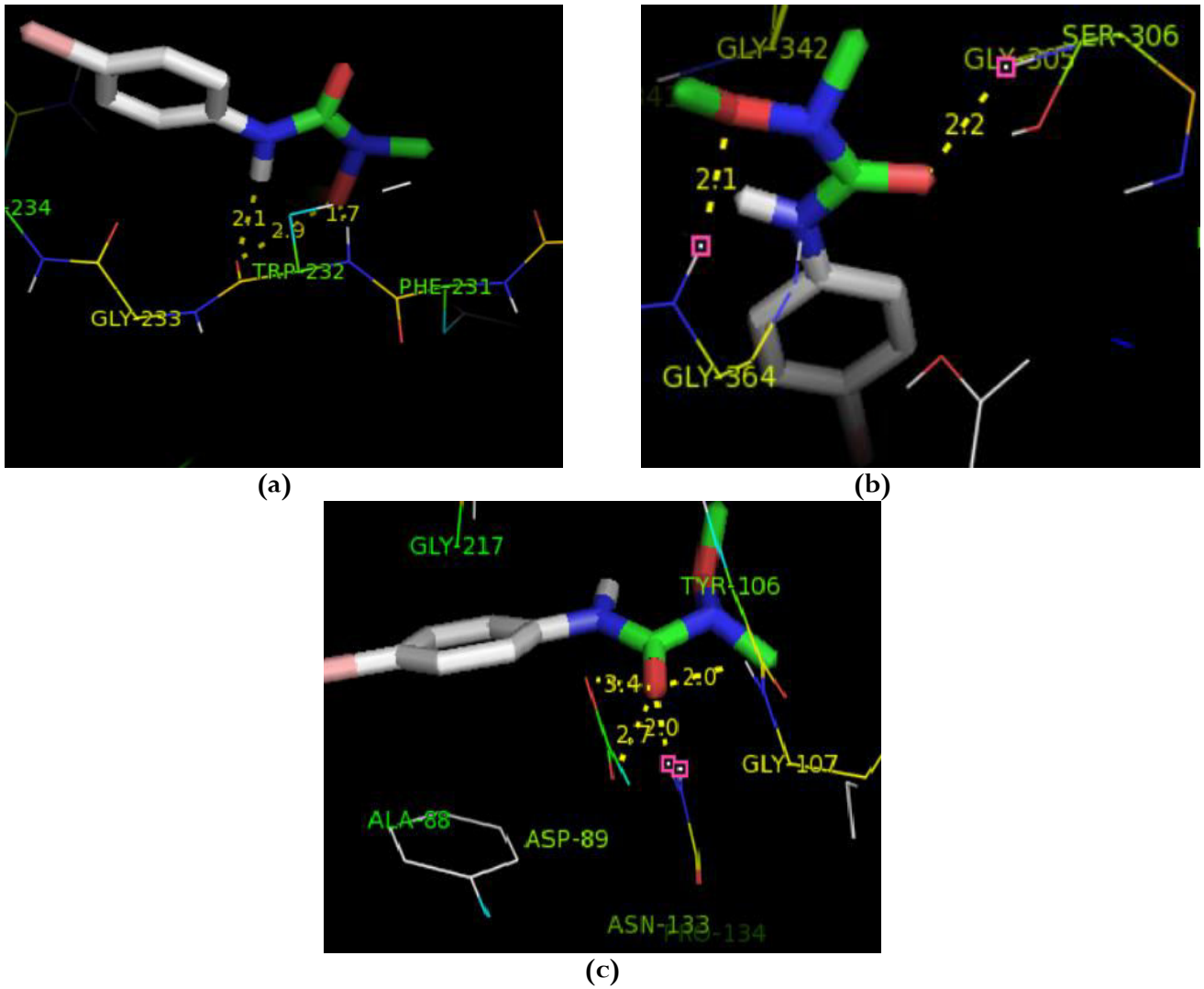


Fig. 6: Interaction of 1UZY, 4MY1, 5HCG with BMM molecule

Table 10: Hydrogen bonding and the molecular docking of BMM with the protein (1UZY, 4MY1, 5HCG)

Protein (PDB ID)	Bond residues	Bond distance [Å]	Inhibition constant [μm]	Binding energy [kcal/mol]	Inter molecular energy [kcal/mol]	Reference RMSD [Å]
1UZY	ASP89 GLY107 ASN133	3.4 2.7 2.0 2.0	117.53	-5.36	-5.96	113.56
4MY1	SER306 GLY364	2.2 2.1	18.43	-6.46	-7.06	24.06
5HCG	TRP232	2.1 2.9 1.7	227.39	-4.97	-5.57	44.03

3.11. Antimicrobial activity of BMM

Agar well diffusion method is widely used to antimicrobial activity of the compound. Muller-Hinton Agar media plates were swabbed (sterile cotton swabs) with 8 hour old - broth culture of respective bacteria. Candida sp. was swabbed on Antimycotic Sensitive media (AMS media). After inoculums, wells with the size of 10 mm diameter and about 2 cm a part were made in each of these plates using sterile cork borer. Stock solution of each drug extract was prepared at a concentration of 1 mg/ml in water. About 100 µl of different concentrations of the given drug solvent extracts were added into the wells and allowed to diffuse at room temperature for 2 hrs. The plates were incubated at 37°C for 24 hrs. After incubation, the diameter of the inhibition zone (mm) was measured and the activity index was also calculated. The antimicrobial activity of the compound is presented in Table 11.

Table 11: Antimicrobial activity of the BMM compound

Pathogens	Zone of inhibition (mm) at 30µl	
	Positive Control (mm)	Size of Inhibition (mm)
Candida Sp.,	25	22
Escherichia coli	23	20

4. CONCLUSION

In this work, the optimized parameters were theoretically determined and compared with the experimental results of the BMM molecule. The shortening of the C-N bond demonstrates the molecules resonance effect. Using NBO analysis, the intramolecular hyperconjugative interactions (N_7-C_9...O_{10} and C_9-N_{11}...O_{10}) are responsible for the molecules stability, which is very important in the enhancement of the antimicrobial activity of the compound. The experimental and theoretical spectroscopic analyses of BMM molecules using FT-IR, FT-Raman, and UV-Vis are reported in this study, and the theoretical and experimental values are compared. NBO analysis was used to calculate the intramolecular interaction and electron density. The electronic properties of the BMM molecule, with a HOMO-LUMO energy gap of 5.3775 eV, indicate antimicrobial activity. Molecular electrostatic potential surface analysis and Fukui function analysis were used to predict the active sites for electrophilic and nucleophilic attacks. It confirms that the area around the oxygen atom has a high electron density and that the atoms are bound with positively charged proton. Global Reactivity Descriptors for a selected atomic site in BMM explains the antimicrobial activity. The BMM molecule reveals more biological activity nature due to higher value of electrophilicity index (ω=2.3102).The NLO values indicate that BMM could be used to create electronic and opto-electronic devices. The lowest binding energy of protein 5HCG are docked with the molecule of BMM is more effective and shows more antimicrobial activity. The antimicrobial activity results of the viability assay have proved that BMM molecule possess excellent antifungal and antibacterial nature since fungi and bacteria cannot grow in the media containing BMM molecule. The lowest concentration of antimicrobial drug that was sufficient to inhibit microbial growth the MIC. Thus from above investigations, it can be concluded the BMM molecule is a good antimicrobial agent to treat diseases and further work can be responsible for biological activity.

5. ACKNOWLEDGEMENT

The Authors thank Dr. I. Hubert Joe, Associate Professor of Department of Physics and Kerala University for granting us permission to do computational works in their Research Lab.

Declaration of competing interest

The authors declare that they have no known competing financial interests or personal relationships that could have appeared to influence the work reported in this paper.

6. REFERENCES

1. Oettmeier W. *Cell Mol Life Science,* 1999; **55:**1255-1256.
2. Benitez FJ, Garcia C, Acero JL, Real FJ. *W Acad Sci Energy Technol,* 2009; **3**:10-13.
3. Rouchaud J, Metsue M, Van Himme M, Gillet J, Benoit F, Ceustermans N. *Soil Biol Biochem,*1988; **20:** 761-764.
4. Frisch MJ, Trucks GW, Schlegel HB, Scuseria GE, Robb MA, Cheeseman JR et al. *Gauss '09 Revision B*, 2010; **01.**
5. Foresman JB, Pittsburg PA, Frisch E. Exploring Chemical Electronic Structure Methods Gauss'09**,** 1996.

6. Dennington R, Keith T, Millam J. Semi Chemical Inc Shaw Missi Ks Gaussview Ver 5, 2009.
7. Pulay P, Fogarasi G, Pang F, Boggs J E. *J Am Chem Soc,* 1979; **101:**2550-2551.
8. Sundius T. *Vib Spectro*, 2002; **29:**89-91.
9. Vallejos ST, Erben MF, Piro OE, Castellano EE, DellaVedova CO. *P plyhe*, 2009; **28** 937-938.
10. Abraham JP, Sajan D, Hubert Joe I, Jayakumar V S. *Spectro chem Acta Part A,* 2008; **71:**355-356.
11. Smith B. CRC press, 1999.
12. Krishnakumar V, Prabavathi N. *Spectrochim Acta A,* 2010; **77:**238-240.
13. Sajan D, Binoy J, Joe IH, Jayakumar VS, Zaleski J. *J Raman Spectroscopy,* 2005; **36:**221-223.
14. Lin-Vein D, Colthup N, Fateley WG, Grasselli JG. Academic Press, 1991.
15. Socrates G. Wiley International Science Publications, 1990.
16. Vijayakumar T, Hubert Joe I, Reghunadhan Nair C P, Jayakumar VS. *Chemical Physics,* 2008. **343:**83-85.
17. Al Alshaikh MA, Sheena Mary Y, Yohannan Panicker C, Attia MI, Elemam AA ,Van alseynoy C. *J mole struct,* 2016; **1109:**131-134.
18. Tamer O, Sefa Atalay A, Avci D, Atalay Y, Tarcan E, Marchewka MK. *Mater Sci Po*l, 2016; **34**:192-194.
19. Silverstein RM, Webster FX. J Wil and Science Inc, 2003.
20. Mooney EF. *Spectro Acta,* 1964; **20:**1343-1345.
21. Daly LH, Wiberly SE. Acadamic Press NewYork, 1990.
22. Krishnakumar V, John Xavier R. *Spectro Acta A,* 2005; **61:** 253-255.
23. Krishnakumar V, Dhevamalar S, Xavier R J, Balachandran V. *Spectro Acta A,* 2006; **65:**147-149.
24. Young D C. *Comput Chemi A*, 2001;
25. Jacob George, Prasana JC, Muthu S, Tintu KK. *Inter J Mate Sci,* 2017; **12:** 302-305.
26. Parr RG, Pearson RG. *J Am Chem Soc,* 1983; **105:**7512-7514.
27. Meenakshi R. *J Mol Struct,* 2017; **1127:** 694-696.
28. Vural H, Orbay M. *J Mol Struct,* 2017; **1146:**669-971.
29. Guo L, Ren X, Zhou Y, Xu S, Gong Y, Zhang S. *Arab J Chem*, 2017; **10:**121-123.
30. Wazzan N, Mahgoub F. *Open J Phy Chem,* 2014; **4:** 6-8.
31. Koster A M, Leboeuf M, Salahub D R. *Theo Comput Chem,* 1996; **3:**105-107.
32. Majumdar D, Das S, Thomas R, Ullah Z, Sreejith S S, Das D et al. *Inorg Chem Act,* 2019; **492:**221-223.
33. Parameswara Rao K, Rao M C. *Inter J Chemi Sci,* 2016; **14**:2389-2391.
34. Weinhold F, Landis CR. *Chem Educ Res Pract Eur,* 2001; **2:**91-93.
35. Rachelin Y P, Pradhan S, James C. *Spectro Let,* 2018; **51:**144-145.
36. Sebastian S, Sundaragenesan N. *Spectrochim Acta A,* 2010; 75-77.
37. Pathak S, Kumar A, Tandon P. *J Mol Struct*, 2010; **981:**1-3.
38. Morell C, Grand A, Labbe AT. *J Phys Chem A,* 2005; **109:**205-207.
39. Parr RG, Yang W. Oxford University Press New York, 1989.
40. Roy RK, Krishnamurti S, Geerling P, Pal S. *J Phys Chem A,* 1998; **102:**3746-3748.
41. Elamurugu Porchelvi E, Muthu S. *Spectro Acta Part A Mol and Biomol Spectro,* 2015; **134**:453-455.
42. Morries GM, Huey R, Lindstrong W, Scanner MF, Belew RK, Goodsell DS et al. *J Comput Chem*, 2009; **16:**2785-2787.
43. Chien EY, Liu W, Zhao Q, Katritch V, Han G W, Hanson M A et al. *Select Anta Sci,* 2010; **330:**1091-1093.
44. Katritzky AR, Mu L, Lobanov VS, Karelson M. *J Phys Chemi*, 1996; **100:**10400-10402.